Synthesis, Structure, and Phase Behavior of New Chiral Liquid-Crystalline Polysiloxanes Based on Mesogenic Menthyl Monomers

Bao-Yan Zhang, Jian-She Hu, Shi-Chao Ren, Cong Liu

Center for Molecular Science and Engineering, Northeastern University, Shenyang 110004, People's Republic of China

Received 28 March 2008; accepted 28 September 2008
DOI 10.1002/app.29318
Published online 9 December 2008 in Wiley InterScience (www.interscience.wiley.com).

ABSTRACT: Six new chiral monomers ($\mathbf{M_1}$–$\mathbf{M_6}$), and their corresponding side chain polymers ($\mathbf{P_1}$–$\mathbf{P_6}$) containing menthyl groups were synthesized. The chemical structures of $\mathbf{M_1}$–$\mathbf{M_6}$ were characterized with FTIR and ^{1}H NMR. The structure–property relationships of the monomers and polymers obtained are discussed. The mesomorphic properties and phase behavior were investigated by differential scanning calorimetry, thermogravimetric analysis, polarizing optical microscopy, and X-ray diffraction measurements. Some compounds containing menthyl groups formed mesophase when a flexible spacer was inserted between the mesogenic core and the menthyl groups by reducing the steric hindered effect. The monomers $\mathbf{M_1}$, $\mathbf{M_4}$, and $\mathbf{M_5}$ did not reveal mesomorphic properties because of the weaker rigid core or the longer flexible terminal groups, whereas $\mathbf{M_2}$, $\mathbf{M_3}$, and $\mathbf{M_6}$ all revealed cholesteric phase. Except $\mathbf{P_4}$ and $\mathbf{P_5}$, the homopolymers $\mathbf{P_1}$–$\mathbf{P_3}$ and $\mathbf{P_6}$ showed a smectic A phase. In addition, melting, glass transition temperature, or clearing temperature increased, and the mesophase temperature range widened with increasing the rigidity of mesogenic core or decreasing the length of the flexible spacer. © 2008 Wiley Periodicals, Inc. J Appl Polym Sci 111: 3016–3025, 2009

Key words: chiral; liquid-crystalline polymers; menthyl; cholesteric phase; smectic phase

INTRODUCTION

Both from a scientific and a commercial point of view, chiral liquid-crystalline polymers (LCPs) have attracted much interest because of their unique optical and electrical properties, including the selective reflection of light, thermochromism, ferroelectricity, and their potential applications such as optical-electro materials.[1–14] Chirality can be introduced in LCPs at various levels. They are located in the terminal position of the pendant mesogenic units. The rod-like, chiral molecules responsible for the macroscopical alignment of the mesogenic domains can produce a cholesteric or chiral smectic phase. Depending on the chemical structure, it may be feasible to achieve a macroscopic alignment of the chiral mesophase domains. Many side-chain chiral LCPs, mostly adopting commercially available chiral compounds such as cholesterol and (*S*)-(+)-2-methyl-1-butanol, have been studied.[15–23]

Menthol derivatives have been used as a nonmesogenic chiral monomer for the synthesis of side chain chiral LCPs.[24–32] Bobrovsky et al.[26–28] reported some papers with detailed study on the copolymers based on menthyl groups, but in these papers, smectic and cholesteric phases were induced by the introduction of nonmesogenic chiral menthyl monomer into nematic or smectic polymers. Liu and Yang[31] reported synthesis and characterization of novel monomers and polymers containing chiral (−)-menthyl groups. Although these chiral monomers, containing two or three phenyl rings, had good rigidity and tended to reveal a mesophase, their mesogenic cores were directly linked to terminal menthyl groups; thus the existence of the bulky steric menthyl group disturbed the mesogenic arrangement and prevents the development of the LC phases.

However, to the best of our knowledge, research on chiral LC monomers and their corresponding homopolymers directly derived from menthol has been not reported. We found that these monomers and their homopolymers containing menthyl groups could form and exhibit LC phases (such as smectic, cholesteric, or blue phase) when a flexible spacer was inserted between the mesogenic core and the menthyl groups by reducing the steric effect. It is similar to the decoupling effect observed when a flexible spacer is inserted between the polymeric

Correspondence to: B.-Y. Zhang (byzcong@163.com).
Contract grant sponsors: National Natural Science Foundation of China, Program for New Century Excellent Talents (NCET) in University, Science and Technology Bureau of Shenyang.

main chain and the mesogenic side groups. The aims of our research are: (i) to study structure–property relationships of new chiral LC monomers derived from menthol and their corresponding polymers; (ii) to supply the new chiral monomers to synthesize piezoelectric and ferroelectric LC materials. In this study, three chiral LC monomers derived from menthol and their corresponding side-chain polysiloxanes were prepared and characterized. Their mesomorphic properties were investigated with differential scanning calorimetry (DSC), thermogravimetric analysis (TGA), polarizing optical microscopy (POM), and X-ray diffraction (XRD). The structure–property relationships of the monomers and polymers obtained are discussed.

EXPERIMENTAL

Materials

Menthol was purchased from Shanghai Kabo Chemical (Shanghai, China). Allyl bromide was purchased from Beijing Chemical Reagent (Beijing, China). 4-Hydroxybenzoic acid was purchased from Beijing Fuxing Chemical Industry (Beijing, China). 4,4′-Dihydroxybiphenyl (from Aldrich) was used as received. Undecylenic acid was purchased from Beijing Jinlong chemical Reagent (Beijing, China). Polymethylhydrosiloxane (PMHS, $\overline{M}_n$ = 700–800) was purchased from Jilin Chemical Industry. Toluene used in the hydrosilylation reaction was purified by treatment with $LiAlH_4$ and distilled before use. All other solvents and reagents were purified by standard methods.

Measurements

FTIR spectra were measured on a Perkin-Elmer spectrum One (B) spectrometer (Perkin-Elmer, Foster City, CA). ^{1}H NMR (400 MHz) spectra were obtained with a Varian WH-90PFT spectrometer (Varian Associates, Palo Alto, CA). The optical rotations were obtained on a Perkin-Elmer 341 polarimeter. The phase transition temperatures and thermodynamic parameters were determined with a Netzsch DSC 204 (Netzsch, Germany) equipped with a liquid nitrogen cooling system. The heating and cooling rates were 10°C/min. The thermal stability of the polymers under nitrogen atmosphere was measured with a Netzsch TGA 209C thermogravimetric analyzer. The heating rates were 20°C/min. A Leica DMRX POM (Leica, Germany) equipped with a Linkam THMSE-600 (Linkam, England) cool and hot stage was used to observe the phase transition temperatures and analyze the mesomorphic properties through the observation of optical textures. XRD measurements were performed with a nickel-filtered Cu-K_a (λ = 1.542 Å) radiation with a DMAX-3A Rigaku (Rigaku, Japan) powder diffractometer.

Synthesis of the intermediate compounds

The synthesis of the intermediate compounds is outlined in Scheme 1. Menthyloxycarbonylvaleric acid (**2**), 4-allyloxybenzoic acid (**4**), 4-allyloxy-4′-hydroxybiphenyl (**5**), 4-hydroxyphenyl-4′-allyloxybenzoate (**7**), 4-(10-undecylen-1-yloxy) benzoicacid (**9**), 4-hydroxybiphenyl-4′-(10-undecylen-1-ate) (**10**), 4-hydroxyphenyl-4′-(10-undecylen-1-yloxy)benzoate (**12**), and 4-hydroxybiphenyl-4′-(10-undecylen-1-yloxy)benzoate (**13**) were prepared according to the method reported previously.[33–35] Yields, structural characterization, and some physical properties of the intermediate compounds are summarized in Table I.

4-Hydroxybiphenyl-4′-allyloxybenzoate (8)

4-Allyloxybenzoyl chloride **6** was prepared through the reaction of compound **4** with excess thionyl chloride according to the similar reported literature.[34] Compound **6** (19.7 g, 0.1 mol) was dissolved in 50 mL of dry tetrahydrofuran (THF), and then added dropwise to a solution of 4,4′-dihydroxybiphenyl (74.5 g, 0.4 mol) in 200 mL of THF and 20 mL of pyridine. The mixture was reacted for 3 h at room temperature, and then refluxed for 12 h. After removing the solvent by rotatory evaporate, the residue was poured into a beaker filled with 500 mL of water. The crude product was washed several times with 1% NaOH solution, neutralized with chlorhydric acid, washed with hot ethanol, and then recrystallized from acetone. White solid was obtained. Yield 54%, m.p. 219°C. IR (KBr, cm^{-1}): 3445 (—OH); 1707 (C=O); 1642 (C=C); 1604, 1496 (Ar—); 1250 (C—O—C). ^{1}H NMR ($CDCl_3$, TMS): δ 4.65 (d, 2H, —OC***H***$_2$—); 5.03 (s, 1H, —O***H***); 5.32–5.51 (m, 2H, C***H***$_2$=CH—); 6.03–6.10 (m, 1H, CH_2=C***H***—); 7.02–8.15 (m, 8H, Ar—***H***).

Synthesis of the monomers

The synthesis of olefinic monomers is shown in Scheme 2. Six monomers $\mathbf{M_1}$–$\mathbf{M_6}$ were prepared by the same method. The synthesis of $\mathbf{M_1}$ is described below as an example.

4-Allyloxybiphenyl-4′-menthyloxycarbonylvalerate (M_1)

Compound **2** (21.2 g, 0.07 mol) was reacted with 60 mL of thionyl chloride containing a few drops of *N*, *N*-dimethylfomamide for 5 h at 60°C, and then the excess thionyl chloride was removed under reduced pressure to give the corresponding acid chloride. The acid chloride **3** obtained (15.6 g, 0.05 mol) was

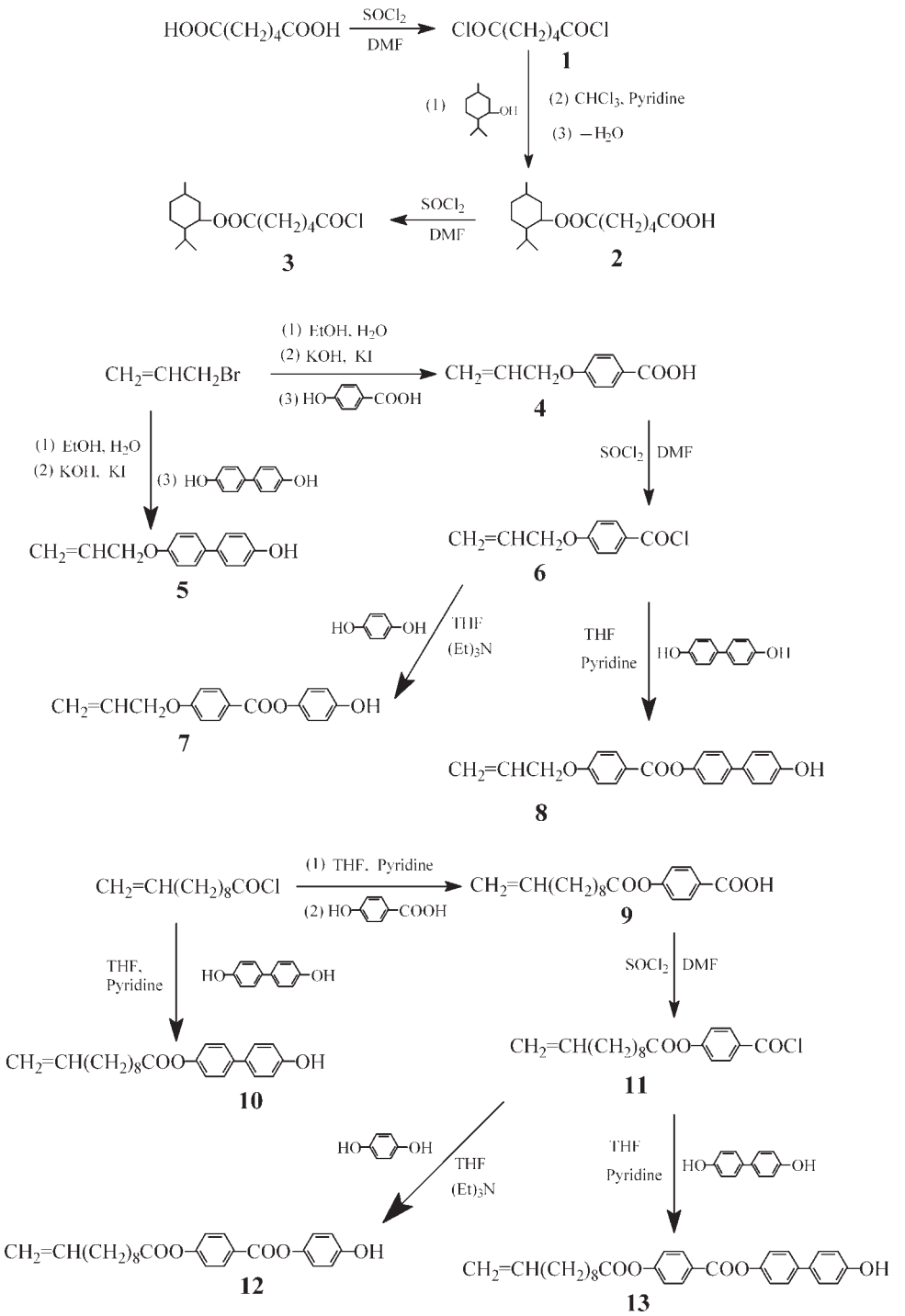

Scheme 1 Synthetic route of intermediate compounds.

dissolved in 20 mL of chloroform, and then added dropwise to a solution of compound **5** (11.3 g, 0.05 mol) in 150 mL of chloroform and 10 mL of pyridine. The mixture was reacted for 6 h at room temperature and refluxed for 30 h, cooled to room temperature and then filtered. After the filtrate was concentrated, the crude product was precipitated by adding methanol to the filtrate, and then recrystallized from ethanol. Yield 75%. $[\alpha]_D^{20}$ −27.9° (toluene). IR (KBr, cm^{-1}): 3077 (=C—H); 2954, 2870 (—CH_3, —CH_2—); 1767, 1739 (C=O); 1643 (C=C); 1606, 1496 (Ar—); 1250 (C—O—C). ^1H NMR ($CDCl_3$, TMS): δ 0.83–2.06 (m, 22H, —OOCCH$_2$C***H***$_2$CH$_2$CH$_2$COO— and menthyl-***H***); 2.25–2.28 (m, 4H, —OOCC***H***$_2$CH$_2$ CH$_2$CH$_2$COO—); 4.05 (m, 1H, —COOC***H***< in menthyl); 4.67 (d, 2H, —OC***H***$_2$—); 5.34–5.55 (m, 2H, C***H***$_2$=CH—); 6.05–6.15 (m, 1H, CH$_2$=C***H***—); 7.01–8.06 (m, 8H, Ar—***H***).

TABLE I
Yield, Melting Temperatures, and IR Characterization of Intermediate Compounds

Compounds	Yield (%)	Recrystallized solvent	T_m (°C)	IR (KBr) (cm^{-1})
2	57	Ethyl acetate	140	3300–2500 (—COOH); 2959, 2874 (CH_3—, —CH_2—); 1751, 1687 (C=O)
4	65	Ethanol	164	3300–2500 (—COOH); 1682 (C=O); 1644 (C=C); 1604, 1450 (Ar—); 1251 (C—O—C)
5	51	Ethanol/acetone (2 : 1)	176	3401 (—OH); 1645 (C=C); 1609, 1512 (Ar—); 1246 (C—O—C)
7	87	Ethanol	148	3421 (—OH); 1706 (C=O); 1643 (C=C); 1605, 1512 (Ar—); 1257 (C—O—C)
9	76	Ethanol	130	3300–2500 (—COOH); 2975, 2852 (—CH_2—); 1754, 1684 (C=O); 1642 (C=C); 1602, 1508 (Ar—)
10	79	Ethanol/acetone (3 : 1)	124	3345 (—OH), 2973, 2852 (—CH_2—), 1756 (C=O), 1641 (C=C), 1605, 1503 (Ar—)
12	55	Ethanol	93	3349 (—OH), 2925, 2852 (—CH_2—), 1758, 1714 (C=O), 1643 (C=C), 1603, 1454 (Ar—)
13	49	Acetone	178	3378 (—OH), 2921, 2849 (—CH_2—), 1754, 1730 (C=O), 1642 (C=C), 1602, 1508 (Ar—)

4-Allyloxybenzoyloxyphenyl-4′-menthyloxycarbonyl-valerate (M_2)

Recrystallized from ethanol. Yield 58%. $[\alpha]_D^{20}$ −38.3° (toluene). IR (KBr, cm^{-1}): 3079 (=C—H); 2924, 2868 (—CH_3, —CH_2—); 1766, 1745, 1732 (C=O); 1644 (C=C); 1607, 1509 (Ar—); 1259 (C—O—C). ^{1}H NMR ($CDCl_3$, TMS): δ 0.85–2.05 (m, 22H, —OOCCH$_2$C***H***$_2$ CH$_2$CH$_2$COO— and menthyl-***H***); 2.25–2.27 (m, 4H, —OOCC***H***$_2$CH$_2$CH$_2$CH$_2$COO—); 3.99 (m, 1H, —COOC***H***< in menthyl); 4.67 (d, 2H, —OC***H***$_2$—); 5.33–5.51 (m, 2H, C***H***$_2$=CH—); 6.04–6.16 (m, 1H, CH$_2$=C***H***—); 6.98–8.19 (m, 8H, Ar—***H***).

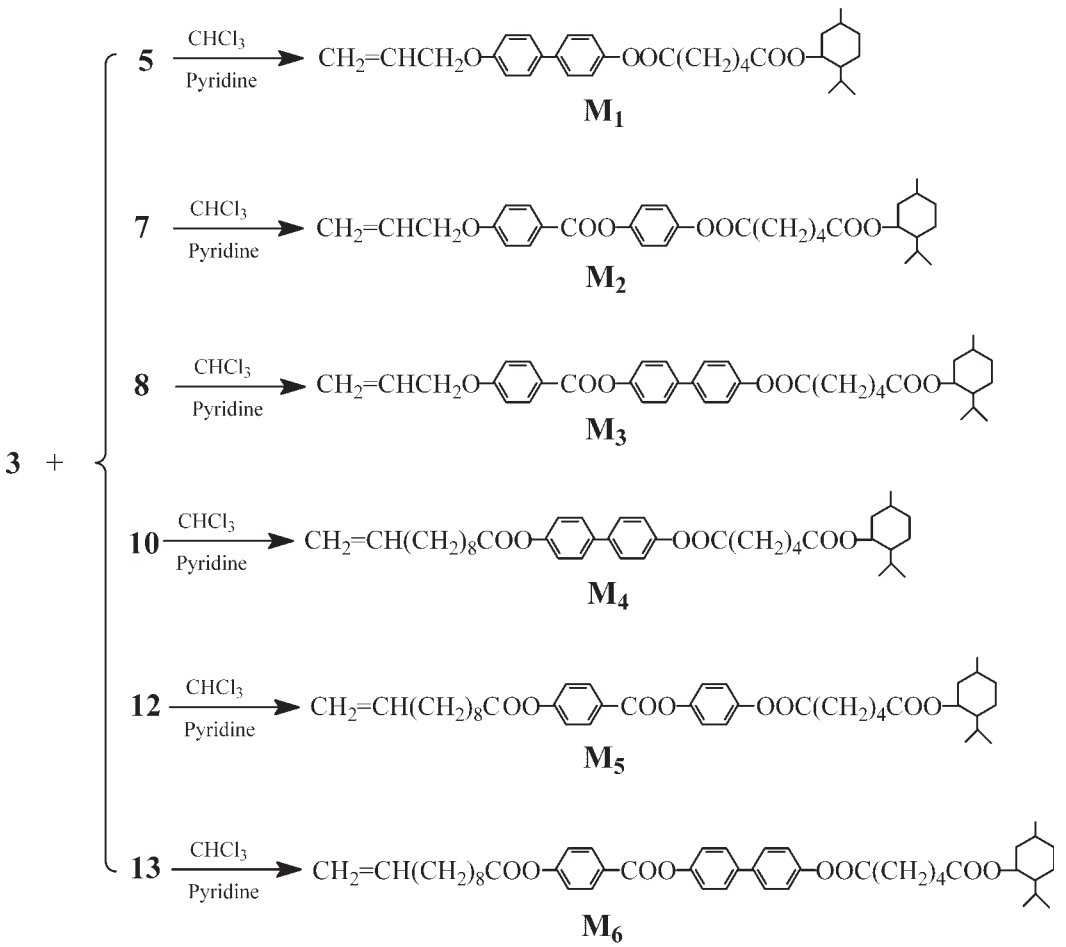

Scheme 2 Synthesis of chiral monomers.

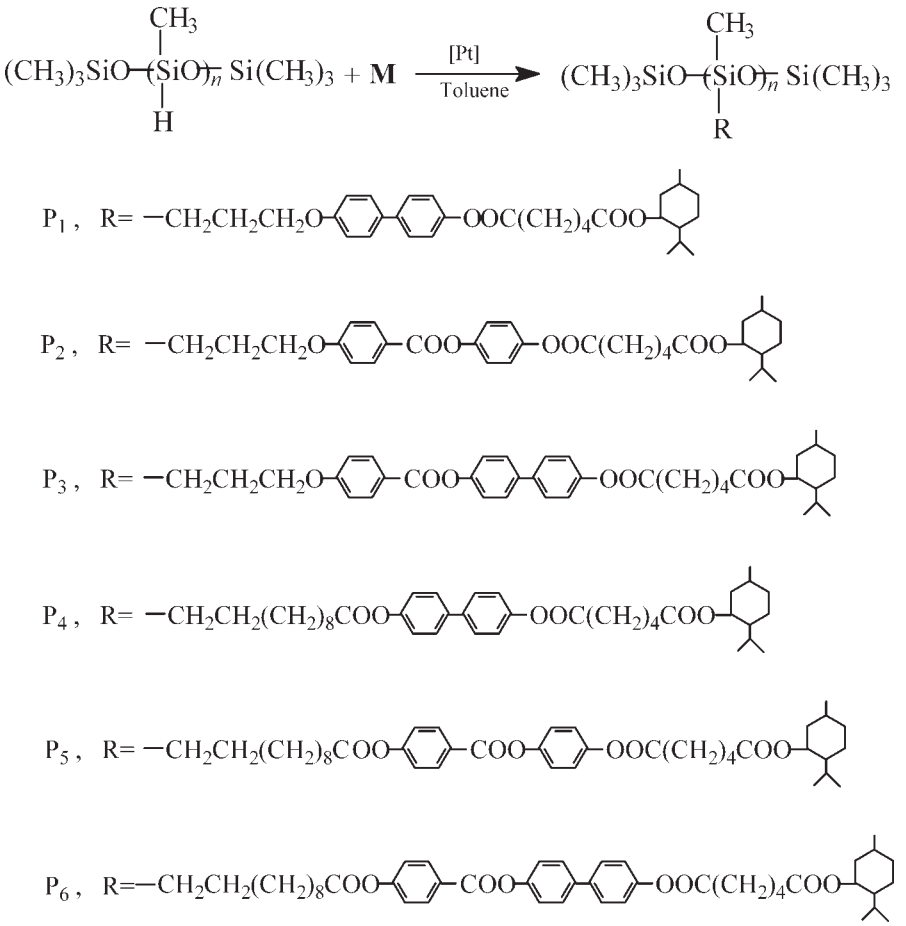

Scheme 3 Synthesis of chiral polymers.

4-Allyloxybenzoyloxybiphenyl-4′-menthyloxycarbonylvalerate (M_3)

Recrystallized from ethanol/acetone (2 : 1). Yield 72%. $[\alpha]_D^{20}$ −21.0° (toluene). IR (KBr, cm^{-1}): 3068 (=C—H); 2982, 2880 (—CH_3, —CH_2—); 1756, 1745, 1721 (C=O); 1642 (C=C); 1605, 1493 (Ar—); 1255 (C—O—C). ^{1}H NMR ($CDCl_3$, TMS): δ 0.84–2.03 (m, 22H, —OOCCH$_2$C***H***$_2$CH$_2$CH$_2$COO— and menthyl-***H***); 2.23–2.25 (m, 4H, —OOCC***H***$_2$CH$_2$CH$_2$CH$_2$COO—); 3.95 (m, 1H, —COOC***H***< in menthyl); 4.66 (d, 2H, —OC***H***$_2$—); 5.36–5.52 (m, 2H, C***H***$_2$=CH—); 6.06–6.13 (m, 1H, CH$_2$=C***H***—); 7.01–8.21 (m, 12H, Ar—***H***).

4-(10-Undecylen-1-yloxy)biphenyl-4′-menthyloxycarbonylvalerate (M_4)

Recrystallized from ethanol. Yield 68%. $[\alpha]_D^{20}$ −29.1° (toluene). IR (KBr, cm^{-1}): 3081 (=C—H); 2954, 2851 (—CH_3, —CH_2—); 1749, 1729, 1721 (C=O); 1640 (C=C); 1604, 1495 (Ar—). ^{1}H NMR ($CDCl_3$, TMS): δ 0.83–2.26 [m, 42H, —(C***H***$_2$)$_8$—, —OOC(C***H***$_2$)$_4$COO— and menthyl-***H***); 4.08 (m, 1H, —COOC***H***< in menthyl); 4.95–5.07 (m, 2H, C***H***$_2$=CH—); 5.79–5.86 (m, 1H, CH$_2$=C***H***—); 7.14–8.21 (m, 8H, Ar—***H***).

4-(10-Undecylen-1-yloxybenzoyloxy)phenyl-4′-menthyloxycarbonylvalerate (M_5)

Recrystallized from ethanol. Yield 66%. $[\alpha]_D^{20}$ −34.1° (toluene). IR (KBr, cm^{-1}): 3068 (=C—H); 2926, 2853 (—CH_3, —CH_2—); 1758, 1745, 1732 (C=O); 1641 (C=C); 1604, 1506 (Ar—). ^{1}H NMR ($CDCl_3$, TMS): δ 0.94–2.25 [m, 42H, —(C***H***$_2$)$_8$—, —OOC(C***H***$_2$)$_4$COO— and menthyl-***H***); 4.07 (m, 1H, —COOC***H***< in menthyl); 4.93–5.06 (m, 2H, C***H***$_2$=CH—); 5.80–5.89 (m, 1H, CH$_2$=C***H***—); 7.05–8.25 (m, 8H, Ar—***H***).

4-(10-Undecylen-1-yloxybenzoyloxy)biphenyl-4′-menthyloxycarbonylvalerate (M_6)

Recrystallized from ethanol/acetone (3 : 1). Yield 65%. $[\alpha]_D^{20}$ −25.4° (toluene). IR (KBr, cm^{-1}): 3072 (=C—H); 2927, 2851 (—CH_3, —CH_2—); 1761, 1736, (C=O); 1642 (C=C); 1605, 1498 (Ar—). ^{1}H NMR ($CDCl_3$, TMS): δ 0.93–2.25 [m, 42H, —(C***H***$_2$)$_8$—, —OOC(C***H***$_2$)$_4$COO— and menthyl-***H***); 4.08 (m, 1H, —COOC***H***< in menthyl); 4.94–5.06 (m, 2H, C***H***$_2$=CH—); 5.80–5.86 (m, 1H, CH$_2$=C***H***—); 7.20–8.28 (m, 12H, Ar—***H***).

TABLE II
Phase Transition Temperature (°C) and Enthalpy Changes (J g^{-1}) of Monomers

Monomers	Mesophase and phase transition[a]	
	Heating cycle	Cooling cycle
$\mathbf{M_1}$	K78.3(58.3)I	I66.7(55.2)K
$\mathbf{M_2}$	K102.4(42.5)Ch168.5(2.5)I	I165.6(2.6)Ch69.4(32.6)K
$\mathbf{M_3}$	K113.2(21.7)Ch202.1(1.1)I	I193.4(1.52)Ch78.0(18.2)K
$\mathbf{M_4}$	K 64.5(73.6)I	I59.7(65.7)K
$\mathbf{M_5}$	K76.9(30.7)I	I69.4(23.6)K
$\mathbf{M_6}$	K101.7(46.7)Ch155.7(1.1)I	I152.6(1.2)Ch77.8(36.7)K

[a] K, solid; Ch, cholesteric; I, isotropic.

Synthesis of the polymers

The synthesis of the polymers $\mathbf{P_1}$–$\mathbf{P_6}$ is shown in Scheme 3. They were synthesized through the hydrosilylation reaction. The synthesis of $\mathbf{P_4}$ is presented as an example, $\mathbf{M_4}$ (5 mol % excess versus the Si—H groups in PMHS) and PMHS were dissolved in dry freshly distilled toluene. The reaction mixture was heated to 60°C under nitrogen and anhydrous conditions, and then 3 mL of THF solution with the H_2PtCl_6 catalyst (5 mg/mL) was injected into mixture with a syringe. The progress of the hydrosilylation reaction, monitored by the Si—H stretch intensity, went to completion, as indicated by IR. $\mathbf{P_4}$ was obtained and purified by several reprecipitations from toluene solutions into methanol, and then dried *in vacuo*. IR spectra of $\mathbf{P_4}$ showed the complete disappearance of the Si—H stretching band at 2165 cm^{-1} and olefinic C=C stretching band at 1640 cm^{-1}. Si—C stretching bands appeared at 1259 and 780 cm^{-1}. Characteristic Si—O—Si stretching bands appeared at 1166, 1115, and 1025 cm^{-1}.In addition, the absorption bands of the ester C=O and aromatic still existed.

RESULTS AND DISCUSSION

Thermal behavior of monomers

The thermal properties of the monomers $\mathbf{M_1}$–$\mathbf{M_6}$ were investigated with DSC and POM. Their phase transition temperatures, enthalpy changes, and mesophase types, obtained on the second heating and the first cooling scans, are summarized in Table II. Representative DSC curves of $\mathbf{M_1}$ and $\mathbf{M_2}$ for a comparison are presented in Figures 1 and 2.

DSC curves of $\mathbf{M_1}$, $\mathbf{M_4}$, and $\mathbf{M_5}$ only showed a melting transition and a crystallization transition on heating and cooling cycles. Moreover, POM observation showed that $\mathbf{M_1}$, $\mathbf{M_4}$, and $\mathbf{M_5}$ did not exhibit any mesomorphic property. However, DSC heating thermograms of $\mathbf{M_2}$, $\mathbf{M_3}$, and $\mathbf{M_6}$ not only showed a melting transition, but also a cholesteric to isotropic phase transition. On cooling scan, an isotropic to cholesteric phase transition and a crystallization transition occurred. As seen from the data listed in Table II, the rigidity of the mesogenic core had a considerable influence on the phase behavior of $\mathbf{M_1}$–$\mathbf{M_6}$. For $\mathbf{M_1}$–$\mathbf{M_3}$, $\mathbf{M_1}$ showed the melting temperature

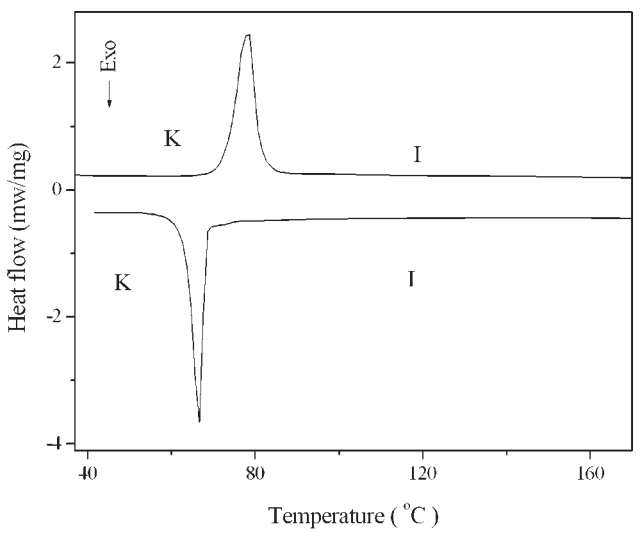

Figure 1 DSC thermograms of $\mathbf{M_1}$.

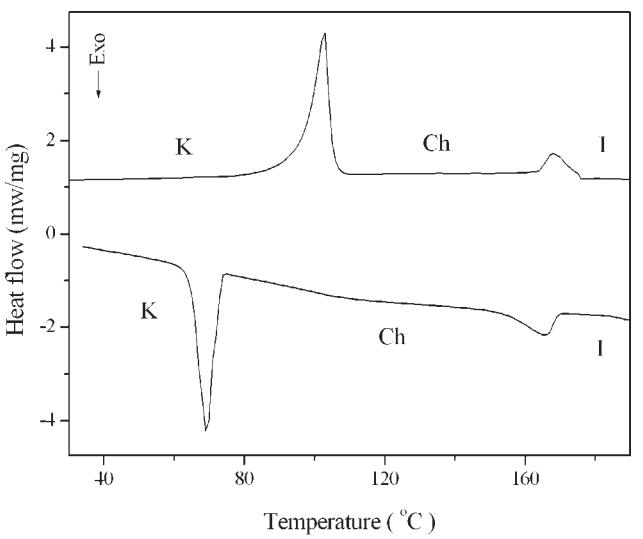

Figure 2 DSC thermograms of $\mathbf{M_2}$.

TABLE III
Specific Rotation, Mesmorphic Properties of Polymers

Polymers	$[\alpha]_D^{20}$	T_g (°C)	T_i[a] (°C)	ΔT[b]	T_d[c] (°C)	Mesophase
$\mathbf{P_1}$	−10.5	43.3	77.8	34.5	322.5	S_A
$\mathbf{P_2}$	−8.2	45.3	172.6	127.3	316.4	S_A
$\mathbf{P_3}$	−17.5	56.8	221.5	164.7	345.3	S_A
$\mathbf{P_4}$	−19.7	16.5	–	–	311.6	–
$\mathbf{P_5}$	−22.2	20.7	–	–	330.2	–
$\mathbf{P_6}$	−9.6	32.4	164.3	131.9	325.7	S_A

[a] Temperature observed with POM.
[b] Mesophase temperature ranges (T_i–T_g).
[c] Temperature at which 5% weight loss occurred.

(T_m), but the isotropic or clearing temperature (T_i) did not appear because of the weaker rigidity of the mesogenic core. With increasing the rigidity of the mesogenic core or the number of phenyl rings in monomer molecules, $\mathbf{M_2}$ and $\mathbf{M_3}$ showed both T_m and T_i. Compared that of $\mathbf{M_1}$, T_m of $\mathbf{M_2}$ and $\mathbf{M_3}$ increased by 24.1 and 34.9°C, respectively. T_i increased from 168.5°C for $\mathbf{M_2}$ to 202.1°C for $\mathbf{M_3}$, moreover, the mesophase temperature ranges widened because T_i increased more than T_m. The reason is that the intermolecular force and the orientational-order increase when the rigidity of the mesogenic core increases. Similarly, $\mathbf{M_4}$ and $\mathbf{M_5}$ only showed T_m, and $\mathbf{M_6}$ showed both T_m and T_i.

The linkage bond in the aryl rings had an influence on the phase transition temperatures for $\mathbf{M_1}$ and $\mathbf{M_2}$, when compared with T_m of $\mathbf{M_1}$, that of $\mathbf{M_2}$ increased because the conjugation action of the ester linkage bond. Moreover, the ester linkage bond also had an influence on the mesomorphic properties, and could make the mesophase appear. $\mathbf{M_1}$ did not show the mesomorphic properties, whereas $\mathbf{M_2}$ revealed the cholesteric phase.

In addition, the flexibility of terminal groups had also an influence on the phase behavior. For example, when compared with $\mathbf{M_2}$ containing allyl terminal group, T_m of $\mathbf{M_5}$ containing undecenyl terminal group decreased by 25.5°C, moreover, the mesomorphic properties of $\mathbf{M_5}$ disappeared because of the better terminal group flexibility.

Thermal analysis of polymers

The thermal properties of the polymers $\mathbf{P_1}$–$\mathbf{P_6}$ were investigated with DSC, TGA, and POM. Their phase transition temperatures, thermal decomposition temperature, and mesophase types are summarized in Table III. Representative DSC curves of $\mathbf{P_2}$ and $\mathbf{P_6}$ are presented in Figure 3. DSC curves of $\mathbf{P_1}$–$\mathbf{P_6}$ all showed the glass transition, but obvious LC to isotropic phase transition did not appear. However, POM results showed that $\mathbf{P_1}$–$\mathbf{P_3}$ and $\mathbf{P_6}$ exhibited the mesomorphic properties. The reason is that bigger viscosity and weaker and slower orientational ability for $\mathbf{P_1}$–$\mathbf{P_3}$ and $\mathbf{P_6}$.

In general, the phase behavior of side-chain LCPs mainly depends on the nature of the polymer backbone, the rigidity of the mesogenic unit, and the length of the flexible spacer. For the polymers $\mathbf{P_1}$–$\mathbf{P_6}$, because of the same polymer backbone, the corresponding phase transition temperatures mainly depend on the rigidity of the mesogenic unit and the length of the flexible spacer in the side groups. The glass transition temperature (T_g) and T_i are very important parameters in connection with structures and properties. With increasing the rigidity of mesogenic units, T_g and T_i increased. For example, T_g increased from 43.3°C for $\mathbf{P_1}$ to 56.8°C for $\mathbf{P_3}$, T_i increased from 77.8°C for $\mathbf{P_1}$ to 221.5°C for $\mathbf{P_3}$, and ΔT increased from 127.3°C for $\mathbf{P_2}$ to 164.7°C for $\mathbf{P_3}$.

Similar to the monomers, the length of the flexible spacer had also an influence on the phase behavior of the polymers. According to Table III, T_g increased from 32.4°C for $\mathbf{P_6}$ to 56.8°C for $\mathbf{P_3}$. T_i also increased from 164.3°C for $\mathbf{P_6}$ to 221.5°C for $\mathbf{P_3}$.

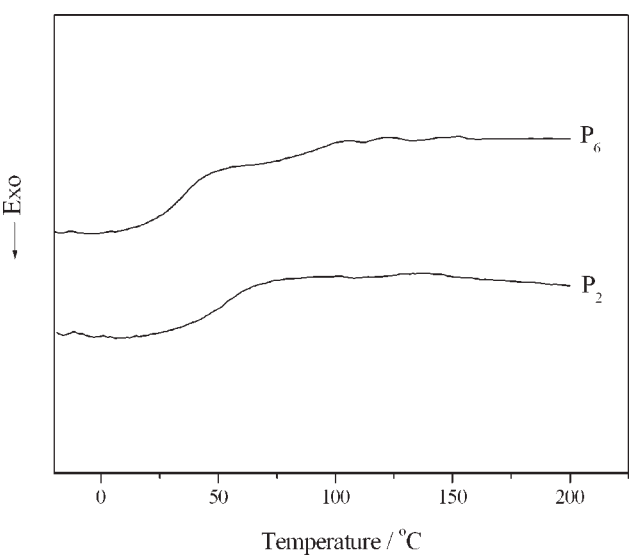

Figure 3 DSC thermograms of $\mathbf{P_2}$ and $\mathbf{P_6}$.

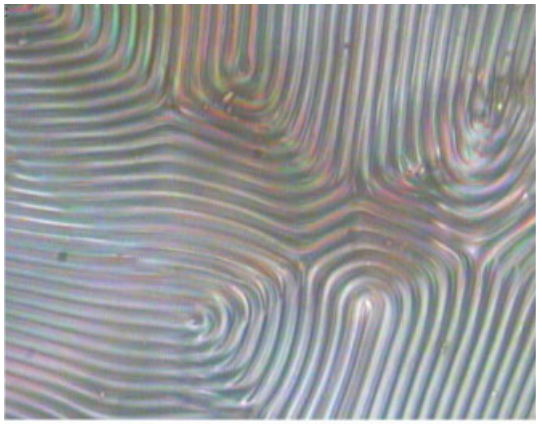

(a) (500×)

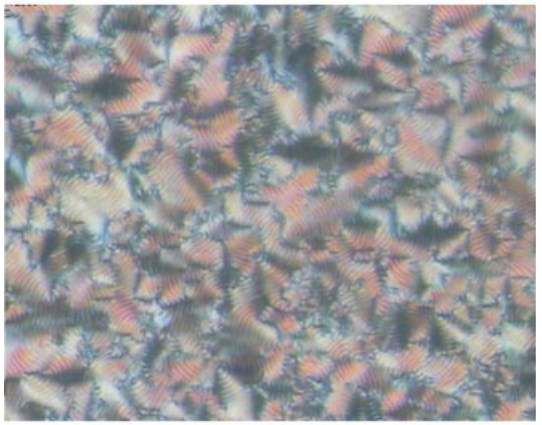

(b) (200×)

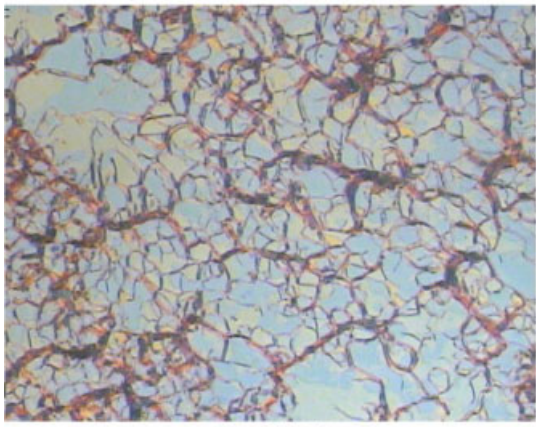

(c) (200×)

Figure 4 Optical textures of monomers. (a) Finger print texture at 154.3°C for $\mathbf{M_2}$; (b) focal conic texture at 130.2°C for $\mathbf{M_3}$; (c) oily streak texture at 146.7°C for $\mathbf{M_6}$. [Color figure can be viewed in the online issue, which is available at www.interscience.wiley.com.]

The thermal stability of $\mathbf{P_1}$–$\mathbf{P_6}$ is detected with TGA. The corresponding data are shown in Table III. TGA results showed that the temperatures at which 5% weight loss occurred (T_d) were greater than 310°C for $\mathbf{P_1}$–$\mathbf{P_6}$; this demonstrated that the synthesized side-chain polymers had good thermal stability. The weight loss rate of $\mathbf{P_1}$–$\mathbf{P_6}$ was very fast from 300 to 400°C. These polymers decomposed about 60% at 400°C.

Textures analysis

The unique optical properties of cholesteric LC materials are related to their helical supermolecular structure. The pitch of helical structure affects texture type of cholesteric phase. In general, if a cholesteric phase has a shorter pitch length, the texture of blue phase or focal conic texture is usually observed; if a pitch length of cholesteric phase lies in the visible range of the spectrum, the planar, oily streak or Grandjean textures are usually observed; if a cholesteric phase has a longer pitch length than the wavelength of visible light, the finger print texture is usually observed.[24,36]

(a)

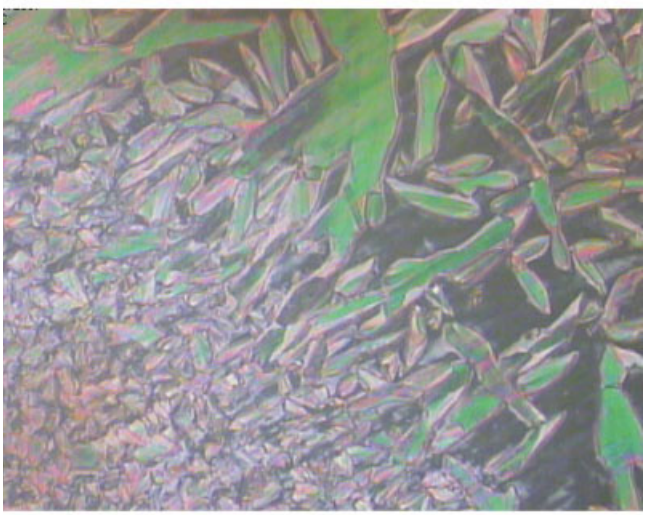

(b)

Figure 5 Optical textures of polymers (×200). (a) batonnet texture at 150.5°C for $\mathbf{P_2}$; (b) batonnet texture at 146.7°C for $\mathbf{P_6}$. [Color figure can be viewed in the online issue, which is available at www.interscience.wiley.com.]

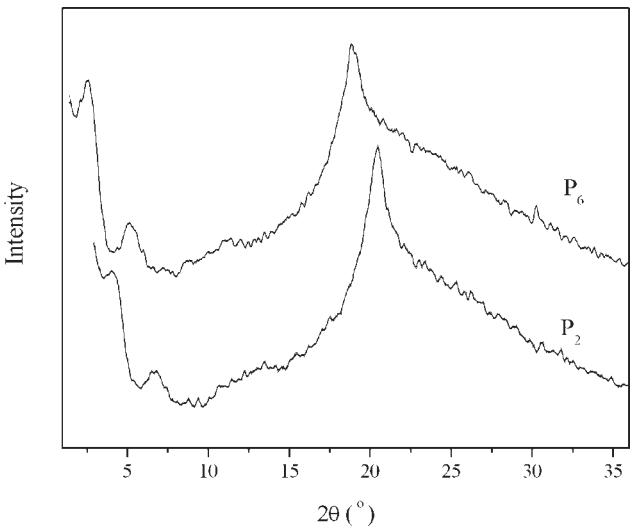

Figure 6 XRD patterns of $\mathbf{P_2}$ and $\mathbf{P_6}$. [Color figure can be viewed in the online issue, which is available at www.interscience.wiley.com.]

The optical textures of $\mathbf{M_1}$–$\mathbf{M_6}$ were observed by POM with a hot stage. $\mathbf{M_1}$, $\mathbf{M_4}$, and $\mathbf{M_5}$ did not show the mesomorphic properties. But $\mathbf{M_2}$, $\mathbf{M_3}$, and $\mathbf{M_6}$ exhibited typical cholesteric oily streak textures, finger print textures with a relatively long pitch, and focal conic textures with a short pitch upon heating and cooling cycles. The phase behavior observed with POM was consistent with DSC results. The optical textures of $\mathbf{M_2}$, $\mathbf{M_3}$, and $\mathbf{M_6}$ are shown in Figure 4(a–c), respectively.

POM results indicated that $\mathbf{P_1}$–$\mathbf{P_3}$ and $\mathbf{P_6}$ all showed the batonnet textures of smectic A (S_A) phase. The optical textures of $\mathbf{P_2}$ and $\mathbf{P_6}$ are shown in Figure 5(a,b). However, the cholesteric phase, exhibited for their corresponding monomers, did not appear. This indicates that the polymer chains hinder the formation of cholesteric helical supermolecular structure of the mesogens, and the mesogenic moieties are ordered in a smectic orientation with their centers of gravity in planes. It is also documented that the mesophase formed by side chain LCPs is more organized than that exhibited by the corresponding monomers.[21] Although $\mathbf{M_1}$ did not reveal any texture, the corresponding polymer $\mathbf{P_1}$ showed the mesomorphic property and the batonnet texture of a S_A phase. This behavior was attributed to an increased density of the mesogenic units in the polymer and hence an organization into the LC phases. In addition, the LCPs with siloxane macromolecular chains tended to form lower order smectic phase, such as a S_A phase.

XRD analysis

XRD studies were carried out to obtain more detailed information on the mesomorphic structure and type. XRD can confirm the presence of the S_A phase. The observed X-ray patterns of $\mathbf{P_1}$–$\mathbf{P_3}$ and $\mathbf{P_6}$ exhibited either one or two sharp reflections. A broad reflection at wide angle (associated with the lateral packings) and a sharp reflection at low angle (associated with the smectic layers) were respectively, shown by XRD curves. Figure 6 shows the XRD curves obtained from powder samples of $\mathbf{P_2}$ and $\mathbf{P_6}$. Their *d*-spacing of the first-order reflection was 21.6 and 34.0 Å, respectively. This gives strong evidence for the formation of the smectic phase. This result is also in agreement with POM results.

CONCLUSIONS

Six new chiral monomers ($\mathbf{M_1}$–$\mathbf{M_6}$) and their corresponding side-chain polymers ($\mathbf{P_1}$–$\mathbf{P_6}$) based on menthol were synthesized and characterized. $\mathbf{M_1}$, $\mathbf{M_4}$, and $\mathbf{M_5}$ did not show any mesomorphic properties because weaker rigidity of mesogenic core, whereas $\mathbf{M_2}$, $\mathbf{M_3}$, and $\mathbf{M_6}$ revealed the oily streak textures, finger print textures, and focal conic textures of the cholesteric phase. $\mathbf{P_1}$ showed the fan shaped texture although its corresponding polymer $\mathbf{M_1}$ did not reveal any texture. In addition, $\mathbf{P_4}$ and $\mathbf{P_5}$ only showed the glass transition, and their mesomorphic properties were not seen. $\mathbf{P_1}$–$\mathbf{P_3}$ and $\mathbf{P_6}$ all displayed the batonnet textures of the S_A phase. Moreover, with increasing the rigidity of mesogenic core or decreasing the length of the flexible spacer, the corresponding T_m, T_g, or T_i increased, and ΔT widened. All of the obtained polymers displayed very good thermal stability.

References

1. Shibaev, V. P.; Plate, N. A. Adv Polym Sci 1984, 60, 174.
2. Broer, D. J.; Lub, J.; Mol, G. N. Nature 1995, 378, 467.
3. Chen, H. P.; Katsis, D.; Mastrangelo, J. C.; Chen, S. H.; Jacobs, S. D.; Hood, P. J Adv Mater 2000, 12, 1283.
4. Rukmani, S.; Ganga, R. J Polym Sci Part A: Polym Chem 2001, 39, 1743.
5. Lin, Q.; Pasatta, J.; Long, T. E. J Polym Sci Part A: Polym Chem 2003, 41, 2512.
6. Oaki, Y.; Imai, H. J Am Chem Soc 2004, 126, 9271.
7. Wang, L.; Wang, X.; Huang, L. J Appl Polym Sci 2004, 92, 213.
8. Kakuchi, R.; Sakai, R.; Otsuka, I.; Satoh, T. Macromolecules 2005, 38, 9441.
9. Abraham, S.; Paul, S.; Narayan, G.; Prasad, S. K.; Jayaraman, N.; Das, S. Adv Funct Mater 2005, 15, 1579.
10. Brettar, J.; Bürgi, T.; Donnio, B.; Guillon, D.; Klappert, R. Adv Funct Mater 2006, 16, 260.
11. Sahin, Y. M. C.; Serhatli, I. E.; Menceloglu, Y. Z. J Appl Polym Sci 2006, 102, 1915.
12. Hsiue, G. H.; Lee, R. H. J Polym Sci Part B: Polym Phys 2006, 44, 2035.
13. Liu, J. H.; Yang, P. C.; Chiu, Y. H.; Suda, Y. J Polym Sci Part A: Polym Chem 2007, 45, 2026.
14. Ohta, R.; Togashi, F.; Goto, H. Macromolecules 2007, 40, 5228.

15. Hsiue, G. H.; Chen, J. H. Macromolecules 1995, 28, 4366.
16. Hsu, C. S.; Chu, P. H.; Chang, H. L.; Hseih, T. H. J Polym Sci Part A: Polym Chem 1997, 35, 2793.
17. Mihaea, T.; Nozuhiro, K.; Funaki, K.; Koide, N. Polym J 1997, 29, 303.
18. Pfeuffer, T.; Kurschner, K.; Strohriegl, P. Macromol Chem Phys 1999, 200, 2480.
19. Chiang, W. Y.; Hong, L. D. J Polym Sci Part A: Polym Chem 2000, 38, 1609.
20. Hu, J. S.; Zhang, B. Y.; He, X. Z.; Cheng, C. S. Liq Cryst 2004, 31, 1357.
21. Soltysiak, J. T.; Czuprýnski, K.; Drzewínski, W. Polym Int 2006, 55, 273.
22. Zheng, Z.; Sun, Y.; Yi. Xu, J.; Chen, B.; Su, Z. Q.; Zhang, Q. J Polym Int 2007, 56, 699.
23. Hu, J. S.; Li, H.; Liu, C.; Zhang, B. Y. J Appl Polym Sci 2008, 107, 1343.
24. Mihara, T.; Nomura, K.; Funaki, K. Polym J 1997, 29, 309.
25. Altomare, A.; Andruzzi, L.; Ciardelli, F.; Gallot, B.; Solaro1, R. Polym Int 1998, 47, 419.
26. Bobrovsky, A. Y.; Boiko, N. I.; Shibaev, V. P. Liq Cryst 2000, 27, 1381.
27. Bobrovsky, A. Y.; Boiko, N. I.; Shaumburg, K.; Shibaev, V. P. Colloid Polym Sci 2000, 278, 671.
28. Bobrovsky, A. Y.; Boiko, N. I.; Shibaev, V. P. Liq Cryst 2001, 28, 919.
29. Lee, Y. K.; Onimura, K.; Tsutsumi, H.; Oishi, T. J Polym Sci Part A: Polym Chem 2000, 38, 4315.
30. Yoshioka, T.; Zahangir, M.; Ogata, T.; Kurihara, S. Liq Cryst 2004, 31, 1285.
31. Liu, J. H.; Yang, P. C. Polymer 2006, 47, 4925.
32. Liu, J. H.; Yang, P. C.; Hung, H. J. Liq Cryst 2007, 34, 891.
33. Hu, J. S.; Ren, S. C.; Zhang, B. Y.; Chao, C. Y. J Appl Polym Sci 2008, 109, 2187.
34. Hu, J. S.; Zhang, B. Y.; Feng, Z. L.; Wang, H. G.; Zhou A. J. J Appl Polym Sci 2001, 80, 2335.
35. Zhang, B. Y.; Hu, J. S.; Yang, L. Q.; He, X. Z.; Liu, C. Euro Polym J 2007, 43, 2017.
36. Dierking, I. Textures of Liquid Crystals; Weinheim, Hagedorm, Germany: Wiley VCH, 2003.